Published in final edited form as:

Mol Cell Biochem. 2018 April ; 441(1-2): 151–163. doi:10.1007/s11010-017-3181-z.

Unprecedented anticancer activities of organorhenium sulfonato and carboxylato complexes against hormone-dependent MCF-7 and hormone-independent triple-negative MDA-MB-231 breast cancer cells

Paul T. Wilder[#1], **David J. Weber**[#1], **Angela Winstead**[#2], **Sabreea Parnell**[#2], **Tiara V. Hinton**[#2], **Monet Stevenson**[#2], **Dipak Giri**[#2], **Samira Azemati**[#2], **Pola Olczak**[#2], **Brent V. Powell**[#2], **Tijesunimi Odebode**[#2], **Solomon Tadesse**[#2], **Yongchao Zhang**[#2], **Saroj K. Pramanik**[#3], **James M. Wachira**[#3], **Sujan Ghimire**[#2], **Pumtiwitt McCarthy**[#2], **Alexis Barfield**[#4], **Hirendra N. Banerjee**[#4], **Chao Chen**[#5], **James A. Golen**[#5], **Arnold L. Rheingold**[#5], **Jeanette A. Krause**[#6], **Douglas M. Ho**[#7], **Peter Y. Zavalij**[#8], **Roosevelt Shaw**[#2], **Santosh K. Mandal**[#2]

[1]Department of Biochemistry and Molecular Biology, Center for Biomolecular Therapeutics & Marlene and Stewart Greenebaum Comprehensive Cancer Center, University of Maryland School of Medicine, Baltimore, MD, USA

[2]Department of Chemistry, Morgan State University, Baltimore, MD, USA

[3]Department of Biology, Morgan State University, Baltimore, MD, USA

[4]Department of Natural, Pharmacy and Health Sciences, Elizabeth City State University – University of North Carolina, Elizabeth City, NC, USA

[5]Department of Chemistry, University of California, San Diego, CA, USA

[6]Department of Chemistry, University of Cincinnati, Cincinnati, OH, USA

[7]Department of Chemistry, Princeton University, Princeton, NJ, USA

[8]Department of Chemistry and Biochemistry, University of Maryland, College Park, MD, USA

[#] These authors contributed equally to this work.

Abstract

Cisplatin and other metal-based drugs often display side effects and tumor resistance after prolonged use. Because rhenium-based anticancer complexes are often less toxic, a novel series of organorhenium complexes were synthesized of the types: $XRe(CO)_3Z$ (*X* = α-diimines and Z = *p*-

Santosh K. Mandal santosh.mandal@gmail.com.

Author contributions The authors' contributions are as follows: Conceptualization: SKM, SKP, and HNB; Synthesis: TO, SP, TVH, SA, MS, DG, PO, BVP, and AW; Characterizations: AW, TO, and ST; Cytotoxicity studies: PTW and DJW; X-ray structure determinations: CC, JAG, ALR, JAK, DMH and PYZ; Structure optimizations: RS; DNA-binding studies: TO, SP, TVH, SA, MS, DG, BVP, AB, YZ, SG, PM and JMW; Writing of the original manuscript: SKM, SKP, HNB, DJW and PTW; Reviewing–editing: DJW, PTW, SKP, AW, HNB, DMH, ALR, YZ, RS and JMW; Final document approval: DJW and SKM.

Compliance with ethical standards

Conflict of interest The authors have no conflicts of interest to declare in this research.

Electronic supplementary material The online version of this article (doi:10.1007/s11010-017-3181-z) contains supplementary material, which is available to authorized users.

toluenesulfonate, 1-naphthalenesulfonate, 2-naphthalenesulfonate, picolinate, nicotinate, aspirinate, naproxenate, flufenamate, ibuprofenate, mefenamate, tolfenamate, N-acetyl-tryptophanate), and their biological properties were examined. Specifically, in hormone-dependent MCF-7 and hormone-independent triple-negative MDA-MB-231 breast cancer cells, the *p*-toluenesulfonato, 1-naphthalenesulfonato, 2-naphthalenesulfonato, picolinato, nicotinato, acetylsalicylato, flufenamato, ibuprofenato, mefenamato, and N-acetyl-tryptophanato complexes were found to be far more potent than conventional drug cisplatin. DNA-binding studies were performed in each case via UV–Vis titrations, cyclic voltammetry, gel electrophoresis, and viscosity, which suggest DNA partial intercalation interaction, and the structure–activity relationship studies suggest that the anticancer activities increase with the increasing lipophilicities of the compounds, roughly consistent with their DNA-binding activities.

Keywords

Organorhenium; Sulfonate; Carboxylate; MCF-7; MDA-MB-231; Breast cancers

Introduction

More than four decades ago, Professor Mark Wrighton at MIT discovered the luminescent properties of $(N^{\frown}N)(CO)_3ReCl$ ($N^{\frown}N$ = α – diimines) [1]. Since then countless papers have been published describing their uses as luminescent sensors [2], in optical switching [3], as molecular materials for nonlinear optics [4], in monitoring polymerizations [5], in labeling DNA or nucleobases [6, 7], etc. In 2000, Yan and coworkers [8] first described the cytotoxic properties of related rhenium (I) hydroxo and alkoxo carbonyl complexes. Now these and similar organorhenium (I) complexes have been established as strong anticancer agents. In a recent review article in the journal “ACS Chemical Biology,” Professor Gasser at the University of Zurich described the “Underestimated Potential of Organometallic Rhenium Complexes as Anticancer Agents” [9]. We embarked on our study on the cytotoxicity of $(N^{\frown}N)(CO)_3ReZ$ (where Z represents sulfonates such as *p*-toluenesulfonates (a.k.a., tosylates) and naphthalenesulfonates, and carboxylates such as picolinates, nicotinates, tryptophanates, carboxylates from nonsteroidal anti-inflammatory drugs (NSAIDs), etc.) many years ago, primarily due to the facile access of these sulfonates and carboxylates from Mandal’s Synthesis [10, 11]. We have observed that many of these complexes are strong anticancer agents (IC_{50} < 2.0 μM) against U-937 lymphoma and BxPC-3 pancreatic cancer cell lines.

Almost half of all patients who receive chemotherapy are treated with cisplatin and other platinum drugs. Despite their tremendous successes, platinum drugs suffer from two drawbacks. They often display severe side effects, and the development of drug resistance often occurs. Likewise, the antiestrogen drug, tamoxifen, is used for patients suffering from ER(+) breast cancer. This drug causes endometrial cancer, and the tumor develops drug resistance upon prolonged usages. Ferrocene is an organometallic compound. Jaouen lab at Ecole Nationale Supérieure de Chimie de Paris synthesized numerous ferrocene derivatives of tamoxifen known as ferrocifens to avoid drug resistance [12]. It was observed that the ferrocifens are not only active on ER(+) breast cancer, but they work on aggressive ER(−)

breast cancer as well. However, there is a possibility of liver damage due to iron overload [13]. Thus, the exploration of other metal centers should be considered via organometallic syntheses methods. One such metal center is the organorhenium scaffold, which is particularly promising because low IC_{50} values can also be achieved (<0.5 μM) and because we [14] and others [15–19] have demonstrated that organorhenium complexes exhibit very low toxicity on normal cells. For these reasons, we have synthesized a variety of organorhenium sulfonato and carboxylato complexes, which include *p*-toluenesulfonato (**TOS**), 1-naphthalenesulfonato (**1NS**), 2-naphthalenesulfonato (**2NS**), picolinato (**PIC**), nicotinato (**NIC**), N-acetyltryptophanato (**TP**), acetylsalicylato (**ASP**), flufenamato (**FN**), ibuprofenato (**IB**), mefenamato (**MF**), tolfenamato (**TF**), and naproxenato (**NP**) complexes. The structural formulas for 12 series of compounds are shown in Fig. 1, and those for the nitrogen-containing polypyridine ligands N⌒N are shown in Fig. 2.

Materials and methods

The starting materials, pentylcarbonato complexes, *fac*-$(CO)_3(N⌒N)ReOC(O)OC_5H_{11}$; were synthesized through procedures described in the literature [10, 11]. The sulfonic and carboxylic acids were commercially available. The cell lines MCF-7, MCF-10A, and MDA-MB-231 were obtained directly from ATCC, and their catalog numbers are HTB-22, CRL-10317, and CRM-HTB-26, respectively. The UV–Vis spectra were recorded at room temperature using a Varian Cary 50 Scan UV–Vis spectrophotometer. FT-IR spectra were recorded using Perkin-Elmer spectrometer Spectrum Two, and FT-NMR spectra were recorded using Bruker Top Spin 400 MHz spectrometer.

Synthesis of the carboxylato and sulfonato complexes, $(N⌒N)(CO)_3ReZ$

The complexes were obtained through Mandal's Synthesis which involves the treatment of a pentylcarbonato complex [10, 11] with a corresponding sulfonic or carboxylic acid. The sulfonic acids used were *p*-toluenesulfonic acid, 1-naphthalenesulfonic acid, and 2-naphthalenesulfonic acid; the carboxylic acids used were picolinic acid, nicotinic acid, N-acetyl-L-tryptophan, acetylsalicylic acid, flufenamic acid, ibuprofen, mefenamic acid, tolfenamic acid, and naproxen. Typically, an equimolar mixture of a pentylcarbonato complex (100 mg) and a sulfonic or carboxylic acid in 15 mL of dichloromethane was allowed to be stirred for several hours. The reaction was monitored through IR spectroscopy. When the reaction was complete, the solution was concentrated on a rotary evaporator. Hexane was added and cooled −5 °C. The yellow–orange crystals were obtained through filtration. The yields range from 90 to 100%. The synthetic procedures havebeen presented at the American Chemical Society National Meetings [10, 11]. The complexes were characterized spectroscopically and in many cases crystallographically. The spectroscopic characterizations of the few highly potent compounds (**TOS7, TOS6, NIC7, 1NS7, 2NS6, PIC7, IB6, PIC6**, and **1NS6)** are presented here. Data for **TOS7**: FT-IR (cm^{-1}, CH_2Cl_2, ν(C≡O)) 2028 (s), 1923 (s), 1903 (s). ^1H NMR (400 MHz, $CDCl_3$) δ 7.86 (s, 2H), 7.67 (s, 2H), 7.61–7.56 (m, 6H), 7.52 (dt, J = 6.6, 2.0 Hz, 4H), 7.45–7.41 (m, 2H), 7.08–7.03 (m, 2H), 3.31 (s, 6H), 2.30 (s, 3H). ^{13}C NMR (101 MHz, $CDCl_3$) δ 195.77 (2C≡O), 192.01 (C≡O), 163.42, 151.38, 148.88, 140.63, 139.55, 135.79, 129.67, 129.44, 129.05, 128.73, 127.21, 126.49, 126.30, 124.35, 31.19, 21.36. Data for **TOS6**: FT-IR (cm^{-1}, CH_2Cl_2,

ν(C≡O)) 2029 (s), 1927 (s), 1905 (s). ^{1}H NMR (400 MHz, $CDCl_3$) d 9.39 (d, *J* = 5.3 Hz, 2H), 8.04 (s, 2H), 7.78 (d, J = 5.3 Hz, 2H), 7.65–7.55 (m, 12H), 7.14–7.09 (m, 2H), 2.34 (s, 3H). ^{13}C NMR (101 MHz, $CDCl_3$) δ 196.34, 192.24, 153.29, 151.74, 147.87, 140.72, 139.73, 135.45, 129.98, 129.55, 129.25, 128.77, 128.76, 126.51, 126.00, 125.56, 21.41. Data for **NIC7**: FT-IR (cm^{-1}, CH_2Cl_2) ν(C≡O) 2020 (s), 1915 (s), 1893 (s), ν(C=O) 1628 (m). ^{1}H NMR (400 MHz, CD_2Cl_2) δ 8.39 (dd, *J* = 4.8, 1.8 Hz, 1H), 8.18 (dd, *J* = 2.1, 0.9 Hz, 1H), 7.94 (s, 2H), 7.77 (s, 2H), 7.64–7.60 (m, 7H), 7.60–7.56 (m, 4H), 7.03 (ddd, *J* = 7.8, 4.8, 0.9 Hz, 1H), 3.47 (s, 6H). ^{13}C NMR (101 MHz, CD_2Cl_2) d 198.40 (2C≡O), 194.55 (C≡O), 169.39 (C=O), 163.63 151.44, 150.90, 150.89, 149.37, 136.65, 136.37, 130.98, 129.96, 129.92, 129.39, 127.40, 126.47, 124.57, 122.73, 31.16 (CH_3). Data for **1NS7**: FT-IR (cm^{-1}, CH_2Cl_2, ν(C≡O)) 2029 (s), 1923 (s), 1904 (s). ^{1}H NMR (400 MHz, CD_2Cl_2) δ 7.86 (dd, *J* = 7.2, 1.3 Hz, 1H), 7.72–7.62 (m, 4H), 7.61–7.57 (m, 1H), 7.57–7.50 (m, 6H), 7.47 (s, 2H), 7.46–7.41 (m, 4H), 7.25 (dd, *J* = 8.2, 7.2 Hz, 1H), 7.17 (ddd, *J* = 8.1, 6.8, 1.2 Hz, 1H), 6.88 (ddd, *J* = 8.4, 6.8, 1.4 Hz, 1H), 3.06 (s, 6H). ^{13}C NMR (101 MHz, CD_2Cl_2) δ 196.47 (2C≡O), 192.24 (C≡O), 163.66, 151.59, 148.94, 138.79, 136.19, 134.04, 131.85, 130.00, 129.94, 129.34, 128.59, 128.34, 127.32, 126.94, 126.84, 126.58, 126.11, 126.06, 124.67, 124.50, 31.56. Data for **2NS6**: FT-IR (cm^{-1}, CH_2Cl_2, ν(C≡O)) 2029 (s), 1926 (s), 1905 (s). ^{1}H NMR (400 MHz, CD_2Cl_2) d 9.20 (d, *J* = 5.3 Hz, 2H), 7.82 (d, *J* = 9.1 Hz, 3H), 7.64–7.56 (m, 4H), 7.54–7.48 (m, 6H), 7.44 (d, *J* = 8.7 Hz, 1H), 7.42–7.31 (m, 6H), 7.16, *J* = 8.6, 1.8 Hz, 1H). ^{13}C NMR (101 MHz, CD_2Cl_2) δ 197.22 (2C≡O), 192.62 (C≡O), 153.68, 152.21, 148.07, 140.92, 135.78, 134.01, 132.49, 130.36, 130.07, 129.55, 129.19, 129.04, 128.25, 127.94, 127.91, 127.20, 126.43, 126.30, 125.84, 123.03. Data for **PIC7:** FT-IR (cm^{-1}, CH_2Cl_2) ν(C≡O) 2020 (s), 1913 (s), 1892 (s), ν(C=O) 1627 (m). ^{1}H NMR (400 MHz, $CDCl_3$) δ 8.37 (dd, *J* = 4.9, 1.8 Hz, 1H), 7.97–7.95 (m, 1H), 7.88 (s, 2H), 7.76 (dt, *J* = 7.8, 1.9 Hz, 1H), 7.68 (s, 2H), 7.58–7.54 (m, 6H), 7.51–7.46 (m, 4H), 7.03 (ddd, *J* = 7.9, 4.8, 0.9 Hz, 1H), 3.45 (s, 6H). ^{13}C NMR (101 MHz, $CDCl_3$) δ 197.51 (2C≡O), 194.08 (C≡O), 169.49, 163.21, 150.96, 150.41, 150.31, 149.01, 136.80, 135.78, 130.66, 129.62, 129.42, 129.03, 126.95, 125.94, 124.20, 122.52, 30.96. Data for **IB6**: FT-IR (cm^{-1}, CH_2Cl_2) ν(C≡O) 2018 (s), 1915 (s), 1889 (s), ν(C=O) 1625 (m). ^{1}H NMR (400 MHz, CD_2Cl_2) δ 9.32 (t, *J* = 5.3 Hz, 2H), 7.90 (s, 2H), 7.66 (dd, *J* = 15.3, 5.3 Hz, 2H), 7.61–7.47 (m, 10H), 6.33 (d, *J* = 8.1 Hz, 2H), 6.23 (d, *J* = 8.1 Hz, 2H), 2.96 (q, *J* = 7.1 Hz, 1H), 1.96 (d, *J* = 7.1 Hz, 2H), 1.48 (sep, 1H), 0.84 (d, *J* = 7.1 Hz, 3H), 0.62 (d, *J* = 6.6 Hz, 6H). δ ^{13}C NMR (101 MHz, CD_2Cl2) d 199.14 (C≡O), 198.95 (C≡O), 194.69 (C≡O), 179.02 (C=O), 153.79, 153.27, 151.38, 151.37, 151.27, 147.93, 147.88, 141.53, 141.52, 138.43, 136.14, 136.11, 130.17, 130.12, 130.05, 129.50, 128.82, 128.70, 128.30, 126.52, 126.00, 125.81, 125.68, 125.46, 47.10, 45.23, 30.37, 22.42, 19.10. Data for PIC6: FT-IR (cm^{-1}, CH_2Cl_2) ν(C≡O) 2929 (s), 1917 (s), 1892 (s), ν (C=O) 1625 (m). ^{1}H NMR (400 MHz, CD_2Cl_2) d 9.54 (d, *J* = 5.3 Hz, 2H), 8.27 (ddd, *J* = 4.8, 1.8, 1.0 Hz, 1H), 7.96 (s, 2H), 7.76 (d, *J* = 5.3 Hz, 2H), 7.55–7.49 (m, 10H), 7.40–7.32 (m, 2H), 6.99 (ddd, *J* = 7.2, 4.7, 1.6 Hz, 1H). ^{13}C NMR (101 MHz, CD_2Cl_2) δ 198.79 (2C≡O), 194.40 (C≡O), 170.60 (C=O), 153.99, 153.81, 153.77, 151.71, 148.91, 148.15, 136.10, 130.18, 130.10, 129.50, 129.07, 126.33, 125.86, 124.53, 124.51. Data for **1NS6**: FT-IR (cm^{-1}, CH_2Cl_2, ν(C≡O)) 2029 (s), 1927 (s), 1904 (s). ^{1}H NMR (400 MHz, CD_2Cl_2) δ 9.03 (d, *J* = 5.3 Hz, 2H), 7.87 (dd, *J* = 7.2, 1.3 Hz, 1H), 7.76 (s, 2H), 7.69–7.43 (m, 15H), 7.25 (dd, *J* = 8.2, 7.2 Hz, 1H), 7.11 (ddd, *J* = 8.1, 6.8, 1.2 Hz, 1H), 6.77 (ddd, *J* = 8.4, 6.8, 1.4 Hz, 1H). ^{13}C NMR (101 MHz, CD_2Cl2) δ 197.08 (2C≡O),

192.62(C≡O), 153.27, 151.82, 147.83, 139.48, 135.78, 133.87, 131.68, 130.31, 130.12, 129.52, 128.67, 128.32, 128.25, 126.71, 126.33, 126.18, 126.08, 125.99, 125.61, 124.70.

DNA-binding studies

UV–Vis titrations

The interactions of **TOS7, TOS6, NIC7, 1NS7, 2NS6, PIC7, IB6, PIC6**, and **1NS6** with CT-DNA (Calf Thymus DNA) have been studied via UV–Vis spectroscopy in order to investigate the possible binding modes to CT-DNA and to calculate the binding constants to CT-DNA (K_b). DMSO stock solution of each complex was diluted with Tris buffer saline at pH 7.2 (5 mM Tris–HCl, 50 mM NaCl), and absorption spectra were recorded in the range of 225–700 nm. Titrations were performed according to the method described earlier [20]. Except for a 75 μM solution of **1NS7**, in all other cases, a 25 μM solution of each complex was titrated with varied amounts of DNA stock solution.

Initially, 3000 μL of the buffer in the reference cuvette and 3000 μL of the buffer in the sample cuvette were diluted with equal amounts of neat DMSO and a DMSO solution of the complex, respectively. During the titrations, a measured amount of DNA was added to each cuvette from the DNA stocksolutionof1693 μM to achieve a desired concentration of the DNA solution in each cuvette. The solutions were mixed thoroughly by repeated inversion and were allowed to incubate for 10 min before the absorption spectra were recorded. The change in concentration of the complexes due to each titration was negligible.

Cyclic voltammetry (CV) studies

The interactions of the complexes with CT-DNA have been also investigated by monitoring the changes observed in the cyclic voltammogram of the complexes upon addition of CT-DNA. All electrochemical studies were performed using a CH Instrument Electrochemical analyzer in a single compartmental cell with a three-electrode configuration comprising a Pt wire as the auxiliary electrode, a glassy carbon electrode as the working electrode, and Ag/AgCl as the reference electrode. A 1:1 mixture of acetonitrile and Tris buffer (pH 7.2) was used as the solvent, and 0.05 M tetrabutylammonium perchlorate as the supporting electrolyte.

Agarose gel electrophoresis

Given that these compounds are fluorescent, potential binding to DNA could be investigated through their ability to stain DNA in agarose gels. The compounds were incubated with lambda bacteriophage *Hin*dIII DNA ladder generated at room temperature for 1 h prior to the addition of 0.1× gel loading buffer (65% sucrose, 10 mM Tris–HCl, pH 7.5, 10 mM EDTA, 0.3% bromophenol blue). Electrophoresis was conducted in TAE buffer as follows. The gels were cast in TAE buffer, pH 8.0 (40 mmM Tris.HCl, pH 8.0, 20 mM acetic acid, and 1 mM EDTA). Electrophoresis was carried at 8 volts/cm constant voltage for 2 h. The gels were preimaged using a VersaDoc molecular imager (BioRad) and then stained with ethidium bromide (**EB**) and imaged.

Viscosity

The interaction of CT-DNA with the complexes has been also studied by measuring the change in viscosity upon addition of CT-DNA to the complexes. CT-DNA was quantitated using a NanoVue UV spectrophotometer at 260 nm. A stock solution of DNA in 5 mM KH_2PO_4 and 4 mM NaCl at pH 7.2 was sheared using a sonicating water bath (Branson) for pulses of—120 s on/30 s off—for a total of 60 min. For binding studies, a constant concentration of 200 lM of DNA was used. Binding to **EB** or compounds were tested using 4, 8, 12, 16, 20, 24, 48, 96, and 200 μM solutions after 30 min of incubation at room temperature. Viscosities of DNA/compound or DNA/**EB** were measured in the same manner using a 3156 viscometer (Q Glass Company Inc). Flow time was measured using a digital stop watch. The flow rate of buffer alone and the flow rate of buffer plus DNA solution were measured as control. Each measurement was done in triplicate, and the average flow rate was calculated. Relative viscosities for the CT-DNA in the presence and absence of the organorhenium complexes were calculated from the relation: $\eta \propto (t - t_o)$, where t is the observed flow time of DNA solutions and t_0 is that of phosphate buffer alone. Data are presented as $(\eta/\eta_0)^{1/3}$ versus [complex]/[DNA], where η is the viscosity of DNA in the presence of the organorhenium complexes and η_0 is the viscosity of DNA alone.

Cytotoxicity assay

The ER(?) MCF-7 breast cancer cell lines (ATCC) were maintained in MEM (Cellgro) supplemented with 0.01 ng/mL insulin (Sigma; human insulin), 10% fetal bovine serum (Gemini Bio-products), and 1% Pen/Strep (Gemini Bioproducts).TheER(−)MDA-MB-231breastcancercelllines (ATCC)were maintained in DMEM (Cellgro)supplemented with 10% fetal bovine serum (Gemini Bio-products) and 1% Pen/Strep (Gemini Bio-products). The ER(−) MCF-10A breast cell lines (ATCC) were maintained in DMEM/F12 (Gibco) supplemented with 5% horse serum (Invitrogen), 20 ng/mL EGF (Sigma), 500 ng/mL Hydrocortisone (Sigma), 100 ng/mL Cholera Toxin (Sigma), 10 mg/mL Insulin (Sigma; human insulin), and 1% Pen/Strep (Gemini Bio-products). On day 1, the cell lines were trypsinized, suspended in their respective media to 25,000 cells/mL, and 40lLwerealiquotedinto384-wellcleartissueculturepla tes for 1000 cells per well. On day 2, 0.5 lL of compound serial diluted in DMSO was added using a Beckman Coulter Biomek FX equipped with a 96-pin V&P Scientific Pin Tool with an equivalent amount of DMSO being added for the “DMSO control.” The cells were incubated at 37 °C and 5% CO_2 until day 5, or 72-h post drug addition, at which time 4 μL of Alamar Blue reagent (Thermo Scientific) was added to each well including top the “DMSO control” wells. The plates were incubated for an additional 2 hat37 °C, and then the fluorescence read withanexcitationof540 ± 10 nm and anemissionof590 ± 10 nm on a PHERAstar FS multimode microplate reader (BMG Labtech). The “percent fluorescence intensity of the DMSO control” was determined from the measured relative fluorescence units (RFUs) as follows: (CMPD RFU/DMSO Control RFU) × 100. The IC_{50} was determined by nonlinear curve fitting to the dose–response curve using Origin 6.1 (OriginLab Corp).

Results and discussion

Synthesis and characterizations

The sulfonato and carboxylato complexes were easily obtained from Mandal's Synthesis which involves the conversion of the parent $Re_2(CO)_{10}$ in the presence of α-Diimine, 1-pentanol and CO_2 to the corresponding pentylcarbonato complex, **A** (Eq. 1):

$$\begin{aligned} &Re_2(CO)_{10} + 2(\,N\frown N\,) + 2\ CH_3(CH_2)_4OH + 2\ CO_2 \\ &\quad\rightarrow 2(CO)_3(\,N\frown N\,)ReOC(O)O(CH_2)_4CH_3(\mathbf{A}) + 4\ CO \\ &\quad + H_2 \end{aligned} \tag{1}$$

and subsequent reactions of **A** with sulfonic or carboxylic acids to afford the corresponding sulfonato or carboxylato complexes (see reference 11) (Eq. 2):

$$\begin{aligned} &(CO)_3(\,N\frown N\,)ReOC(O)O(CH_2)_4CH_3 + HZ \\ &\quad\rightarrow (CO)_3(N\frown N)ReZ + CH_3(CH_2)_4OH + CO_2 \end{aligned} \tag{2}$$

(Z represents *p*-toluenesulfonates, naphthalenesulfonates, picolinates, acetylsalicylates, etc.)

The complexes were characterized through FT-IR and FT-NMR spectroscopic techniques and in some cases through X-ray crystallography. The spectroscopic characterizations of a few lead compounds (**TOS7**, **TOS6**, **NIC7, 1NS7**, **2NS6**, **PIC7**, **IB6**, **PIC6**, and **1NS6**) are described here. All these compounds have facial (fac) geometry. Therefore, the IR spectrum of each exhibits three strong m(C:O)'s in the region of 2030–1890 cm^{-1} (Figs. S1–S9). As expected, each of NIC7, PIC7, IB6, and PIC6 shows a medium intensity ν(C≡O) at ~1630 cm^{-1}. The ^1H NMR spectrum of each complex shows the expected number of protons. ^{13}C NMR data acquisition for each compound was done over a period of 48 h. It seems **IB6** was not stable in CD_2Cl_2 during that long period of time. Except **IB6**, each complex exhibits the expected numbers of C≡O, C=O, aromatic, and aliphatic carbon peaks (Figs. S10–S27). The complexes **TOS7**, **1NS7**, and **2NS-6** were also characterized crystallographically (Fig. 3).

DNA-binding studies

UV–Vis absorption titrations can be used to observe the interaction of transition metal complexes with DNA. When a metal complex binds to DNA by coordination, hyperchromicity is observed. When intercalation takes place between a complex and DNA base pairs, hypochromism and bathochromic shift are observed due to the stacking interaction of the π-orbital of the base pairs and π*-antibonding orbital of the aromatic chromophore. The titration graph for **TOS7** is shown in Fig. 4, and the titration graphs for **TOS6**, **NIC7**, **1NS7**, **2NS6**, **PIC7**, **IB6, PIC6**, and **1NS6** are shown in Figs. S28–S35, respectively. Hypochromic effect is observed for each compound. Similar hypochromic effect was also reported for **TOS5** [21]. The DNA-binding constants (K_b) were determined through the method, which was reported earlier [20]. The K_b values are in the range of 10^4–10^5 M^{-1}, which are significantly lower than that of the classical DNA intercalator **EB** (K_b = 1.4×10^6 M^{-1}) [22]. Because of the relatively low K_b values, it is possible that the compounds follow moderate intercalation interactions with DNA. On the other hand, in the absence of red shifts in the titrations, DNA groove-binding mechanism is another possibility.

Electrochemical investigation on the interaction between a redox compound and a biomolecule provides a useful complement to UV–Visible and other related spectroscopic methods and gives information on the mechanism of formation of the compound–biomolecule adduct. A decrease in the peak current of the redox process suggests the formation of an adduct of the electroactive compound with the biomolecule. In addition, a negative shift of the cathodic potential suggests an external binding of the compound to DNA. Figure 5 depicts the cyclic voltammogram of **1NS6**, and Figs. S36–S43 show the cyclic voltammograms of **2NS6**, **TOS7**, **1NS7**, **TOS6**, **PIC7**, **PIC6**, **IB6**, and **NIC7**, respectively, in the absence and presence of DNA. All complexes have an irreversible oxidation peak between 1.3 and 1.4 V, which is ascribed to the metal-centered one-electron oxidation [23]. Additions of 0.1 mM DNA to **TOS7**, **1NS7**, **TOS6**, **PIC7**, **PIC6**, and **IB6** show virtually no change to the oxidation peak, indicating that there is no or little interactions between the complexes and DNA. To **1NS6** and **2NS6**, addition of DNA significantly reduces the peak intensity suggesting interactions between the complexes and DNA; it is worth noting that addition of DNA to **1NS6** causes cloudiness/precipitate suggesting strong interactions between the compound and DNA. It is interesting to note that addition of DNA to **NIC-7** causes the oxidation peak to increase rather than decrease. The reason for such increase is not clear to us at this moment.

The results of gel electrophoresis DNA-binding assays are shown in Fig. 6. In the experiments, lambda *Hin*dIII DNA markers, which give a characteristic laddering pattern in agarose DNA electrophoresis gels, were mixed with the selected compounds or with DMSO, the vehicle for the compounds. DNA by itself is not fluorescent, but it can be visualized in gels through staining with fluorescent dyes. The results indicate that a subset of these compounds (**TOS6, TOS7**, and **1NS7**) bind to DNA to produce the laddering pattern when imaged under a broad band UV lamp. These results suggest that in some cases, the cytotoxicity may be mediated through DNA binding although other mechanisms cannot be ruled out.

Photophysical and optical probes provide sufficient clues to confirm the binding mode. However, viscosity amounts to hydrodynamic measurements and is considered to be the least ambiguous and the most critical means of studying the DNA-binding mode of metal complexes. Thus, viscosity measurement provides a stronger argument for intercalative binding mode. The effects of the organorhenium complexes and **EB** on the viscosity of CT-DNA are shown in Fig. 7. As illustrated in this figure, upon increasing the concentrations of the organorhenium complexes, the relative viscosities of complexes increase steadily similar to the behavior of **EB**. The increase is attributed to the elongation of DNA polymer by effecting separation of DNA base pairs, which amounts to an increase in overall DNA length to accommodate the bound ligand. The increased degree of viscosity which depends on the binding affinity to DNA is according to the following order: **EB ~PIC7 ~ 2NS6 ~ 1NS7 ~ TOS7> 1NS6 ~ PIC6> NIC7> IB6> TOS6**. These results suggest that the complexes intercalate between the base pairs of DNA. However, a ligand that binds in the DNA grooves causes less-pronounced changes or no change in viscosity of a DNA solution.

It may be suggested from the UV titrations that the complexes either bind to DNA intercalatively or follow DNA groove binding [24]. The CV studies and gel electrophoresis experiments lead us to believe that a few complexes bind to DNA.

Also we have observed that the relative viscosity of DNA increases with the increasing concentration of the organorhenium complexes, and the increase is comparable to the classical intercalator **EB**. We conclude that the organorhenium complexes intercalate to DNA. Because the DNA-binding constant (K_b) values are much lower than that of **EB**, other modes of binding are also operative. We have solved the crystal structures of numerous tosylato, naphthalenesulfonato, picolinato, nicotinato, acetylsalicylato, flufenamato, mefenamato, and naproxenato complexes. The phenanthroline ligand in each complex is planar as evidenced from the X-ray structures of **TOS2, ASP2**, and **NIC4** (Fig. S44) and optimized structures of **NIC7**, **PIC7**, **PIC6**, and **TOS6** (Fig. S45) obtained from DFT calculations. In addition, the X-ray structures of the highly potent compounds such as **TOS7**, **1NS7**, and **2NS6** (Fig. 3) also confirm the planarity of the polypyridyl rings. These facts reinforce the DNA intercalative binding of the rhenium complexes. It is worthwhile to mention here that many rhenium complexes like those observed in our cases bearing planar polypyridyl rings exhibit no intercalation interaction with DNA [25–27].

Cytotoxicity assay

We have studied the cytotoxicity of 12 series of new organorhenium compounds. Each series contains at least 5–6 different compounds. Cell viability assays were carried out through Alamar Blue assay. The fluorescence graphs for each compound on MCF-7A, MCF-10A, and MDAMB-231 are compiled in Table S1. For a few lead compounds, some of the graphs are shown in Fig. 8. As seen from the graphs above, a few of these compounds are highly cytotoxic against breast cancer cells ($IC_{50} < 0.500$ μM). For convenience, the IC_{50} values of very active compounds on MCF-7, MCF-10A, and MDAMB-231 are compiled in Table 1. Data for all compounds can be found in Tables S2 and S3. Table 1 reveals that except for the IB series, the organorhenium complexes of NSAIDs are not very active on breast cancer cells. We have observed that the DNA-binding data are completely unrelated to the cytotoxicity results. We did not find any correlation between the DNA-binding constants (K_b), viscosity graphs, or other experiments (in vitro studies) with the IC_{50} values (in cell—cytotoxicity data).

Conclusion and perspective

In this study, we have observed that the organorhenium complexes interact with DNA intercalatively at least partially. Several compounds are highly cytotoxic against MCF-7A and MDA-MB-231 breast cancer cells. The IC_{50} values in the nM range and low activity on normal cells make these compounds highly attractive for possible applications as anticancer drugs.

At the World Cancer Congress in Paris on November 1, 2016, the reports from the American Cancer Society and Lancet medical journal warned of an explosion in cancer deaths among women, mainly from breast cancer, with a toll of around 5.5 million a year by 2030 [28, 29]. Therefore, it is an urgent necessity to discover breast cancer drugs that exhibit no side effects

and are drug resistance free. The organorhenium compounds, **TOS7**, **PIC4**, **NIC7**, **1NS7**, and **IB6**, easily obtained from Mandal's Synthesis are highly active on MCF-7 and MDA-MB-231 breast cancer cells (IC_{50} in the range of 0.250–1.00 μM). The IC_{50} values of **TOS-7** and **NIC-7** on MDA-MB-231 are 0.248 ± 0.336 and 0.591 ± 0.145 μM, respectively. It is worthwhile to mention here that there is no cure at present for patients suffering from this breast cancer. Besides Jaouen's ferrocifens [16–18], Lippard lab at MIT has synthesized a Re(V) complex bearing a bathophenanthroline ligand that is ligand 6 in this study. This compound exhibits an IC_{50} value of 0.475 ± 0.161 [27]. In the present study, we have explored the structure–activity relationship (SAR) studies for 12 new series of compounds. It is very clear that the rhenium compounds bearing bathophenanthroline (ligand **6**) and bathocuproin (ligand **7**) are remarkably active on breast cancer cells possibly due to the increased lipophilic character of the organorhenium compounds. It is very likely that the lipophilicities of the polypyridyl ligands (N⁀N) in Fig. 2 roughly follow the trend: **7** > **6** > **4** ~ **5** ~ **8** > **3** > **2**. It is, therefore, expected that the lipophilicities of the organorhenium compounds follow similar trend. In fact, Table 1 indicates that the IC_{50} values for several series of compounds decrease with the increasing lipophilicities. For example, the IC_{50} values of the **TOS** series of compounds on MDAMB-231 breast cancer cells follow the trend: **TOS7** < **TOS6** < **TOS4** ~ **TOS5** < **TOS3** < **TOS2** < **TOS1**. Likewise, the IC_{50} values of the 1NS series of compounds on MDA-MB-231 follow the trends: **1NS7** < **1NS6** < **1NS4** < **1NS2** < **1NS1**. Similarly, the IC_{50} values of the TP and NIC series of compounds on MCF-7 follow the trends: **TP7** < **TP6** < **TP4** < **TP3** < **TP2** and **NIC7** < **NIC4** ~ **NIC5** < **NIC3** < **NIC2** < **NIC1**. To the best of our knowledge, examples of such an exhaustive study with organometallic or coordination complexes against MCF-7 and MDA-MB-231 breast cancer cells are scarce.

Supplementary Material

Refer to Web version on PubMed Central for supplementary material.

Acknowledgements

This research was partially supported by the NCI disability supplement, and the NIH Grant No. T34 GM100831 to HNB and the NIH Grant No. G11HD038439; and Nuclear Regulatory Commission Grant No. NRC-HQ-12-G-27–0086 to SKM. The work was also supported, in part, with funds from the Center for Biomolecular Therapeutics (CBT) at the University of Maryland, School of Medicine (from DJW).

References

1. Wrighton M, Morse DL (1974) The nature of the lowest excited state in tricarbonyl-chloro-1,10-phenanthrolinerhenium(I) and related complexes. J Am Chem Soc 96(4):998–1003
2. Sacksteder L, Lee M, Demas JN, DeGraff BA (1993) Long-lived, highly luminescent rhenium(I) complexes as molecular probes: intra and intermolecular excited-state interactions. J A Chem Soc. 115:8230–8238
3. Yam VWW, Lau VCY, Cheung KK (1995) Synthesis, photophysics and photo-chemistry of novel luminescent rhenium (I) photoswitchable materials. J Chem Soc Chem Commun 2:259–261
4. Ehler TT, Malmberg N, Carron K, Sullivan BP, Noe LJ (1997) Studies of organometallic self-assembled monolayers on Ag and Au using surface Plasmon spectroscopy. J Phys Chem B. 101:3174–3180

5. Kotch TG, Lees AJ, Fuerniss SJ, Papathomas K, Snyder IRW (1993) Luminescence rigidochromism of fac-tricar-bonylchloro(4,7-diphenyl-1,10-phenanthroline)rhenium as a spectroscopic robe in monitoring polymerization of photosensitive thin films. Inorg Chem 32:2570–2575
6. Stoeffler HD, Thornton NB, Temkin SL, Schanze KS (1995) Unusual photophysics of a rhenium(I) dipyridophenazine complex in homogeneous solution and bound to DNA. J Am Chem Soc 117:7119–7128
7. Oriskovich TA, White PS, Thorp HH (1995) Luminescent labels for purine nucleobases: electronic properties of guanine bound to rhenium(I). Inorg Chem 34:1629–1631
8. Yan YK, Cho SE, Shaffer KA, Rowell JE, Barnes BJ, Hall IH (2000) Cytotoxicity of rhenium(I) alkoxo and hydroxo carbonyl complexes in murine and human tumor cells. Pharmazie 55:307–313 [PubMed: 10798247]
9. Leonidova A, Gasser G (2014) Underestimated potential of organometallic rhenium complexes as anticancer agents. ACS Chem Biol 9:2180–2193 [PubMed: 25137157]
10. Mbagu MK, Kebulu DN, Winstead A, Pramanik SK, Banerjee HN, Iwunze MO, Wachira JM, Greco GE, Haynes GK, Sehmer A, Sarkar FH, Ho DM, Pike RD, Mandal SK (2012) Fac-Tricarbonyl(pentylcarbonato)(a-diimine)rhenium complexes: one-pot synthesis, characterization, fluorescence studies, and cytotoxic activity against human MDA-MB-231 breast, CCl-227 colon and BxPC-3 pancreatic carcinoma cell lines. Inorg Chem Commun 21:35–38
11. The synthetic procedure has been presented at the American Chemical Society National Meetings and can be accessed through the Technical Programming Archive: Past National Meetings (2004-present) and the link is: http://www.acs.org/content/acs/en/meetings/nationalmeetings/programarchive.html?_ga=1.29689146.464482569.1442729062
12. Parson C, Smith V, Krauss C, Banerjee HN, Reilly C, Krause JA, Wachira JM, Giri D, Winstead A, Mandal SK (2013) The effect of novel rhenium compounds on lymphosarcoma, PC-3 prostate and myeloid leukemia cancer cell lines and an Investigation on the DNA binding properties of one of these compounds through electronic spectroscopy. J Bioproces Biotechniq. 4:1–5
13. Wang W, Yan YK, Andy Hor TS, Vittal JJ, Wheaton JR, Hall IH (2002) Synthesis, X-ray structures, and cytotoxicity of rhenium(I) carbonyl 2-(dimethylamino)-ethoxide complexes. Polyhedron 21:1991–1999
14. Kumar CA, Carthikeyan S, Varghese B, Veena V, Sakthivel N, Manimaran B (2014) Synthesis, characterization and cytotoxicity evaluation of rhenium(I) based ester functionalized dinuclear metallacyclophanes. J Organomet Chem 766:86–94
15. Ye R-R, Tan C-P, Chen MH, Hao L, Ji LN, Mao Z-W (2016) Mono- and dinuclear phosphorescent rhenium(I) complexes: impact of subcellular localization on anticancer mechanisms. Chem Eur J 22:7800–7809 [PubMed: 27106876]
16. Dallagi T, Saidi M, Vessieres A, Huche M, Jaouen G, Top S (2013) Synthesis and antiproliferative evaluation of ferrocenyl and cymantrenyl triaryl butene on breast cancer cells. biodistribution study of the corresponding technetium-99 m tamoxifen conjugate. J Organomet Chem 734:69–77
17. Cazares-Marinero JJ, Top S, Vessieres A, Jaouen G (2013) Synthesis and antiproliferative activity of hydroxyferrocifen hybrids against triple-negative breast cancer cells. Dalton Trans 43:817–830
18. Cázares-Marinero JJ, Buriez O, Labbe E, Top S, Amatore C, Jaouen G (2013) Synthesis, characterization, and antiproliferative activities of novel ferrocenophanic suberamides against human triple-negative MDA-MB-231 and hormone-dependent MCF-7 breast cancer cells. Organometallics 32:5926–5934
19. Medley J, Payne G, Banerjee HN, Giri D, Winstead A, Wachira JM, Krause JA, Shaw R, Pramanik SK, Mandal SK (2015) DNA-binding and cytotoxic efficacy studies of organorhenium pentylcarbonate compound. Mol Cell Biochem 398:21–30 [PubMed: 25262122]
20. Banerjee HN, Boston A, Barfield A, Stevenson M, Sarkar FH, Giri D, Winstead A, Krause JA, Mandal SK (2016) A study of the effects of novel rhenium compounds on pancreatic and prostate cancer cell lines. Int J Sci Res. 5(7):481–483
21. Dimitrakopoulou A, Dendrinou-Samara C, Pantazaki AA, Alexiou M, Nordlander E, Kessissoglou DP (2008) Synthesis, structure and interactions with DNA of novel tetranuclear, [Mn4(II/II/II/IV)] mixed valence complexes. J Inorg Biochem 102(4):618–628 [PubMed: 18055016]

22. Waring MJ (1965) Complex formation between ethidium bromide and nucleic acids. J Mol Biol 13:269–282 [PubMed: 5859041]

23. Bullock JP, Carter E, Johnson R, Kennedy AT, Key SE, Kraft BJ, Saxon D, Underwood P (2008) Reactivity of electrochemically generated rhenium (II) tricarbonyl a-diimine complexes: a reinvestigation of the oxidation of luminescent Re(CO)3(α-diimine)Cl and related compounds. Inorg Chem 47(17):7880–7887 [PubMed: 18681426]

24. Kaplanis M, Stamatakis G, Papakonstantinou VD, ParavatouPetsotas M, Demopoulos CA, Mitsopoulou CA (2014) Re(I) tricarbonyl complex of 1,10-phenanthroline-5,6-dione: DNA binding, cytotoxicity, anti-inflammatory and anti-coagulant effects towards platelet activating factor. J Inorg Biochem 135:1–9 [PubMed: 24632342]

25. Ma D-L, Che C-M, Siu F-M, Yang M, Wong K-Y (2007) DNA binding and cytotoxicity of ruthenium(II) and rhenium(I) complexes of 2-amino-4-phenylamino-6-(2-pyridyl)-1,3,5-triazine. Inorg Chem 46:740–749 [PubMed: 17257015]

26. Mitsopoulou CA, Dagas C (2010) Synthesis, characterization, DNA binding, and photocleavage activity of oxorhenium (V) complexes with a-diimine and quinoxaline ligands. Bioinorg Chem Appl. doi:10.1155/2010/973742

27. Suntharalingam K, Awuah SG, Bruno PM, Johnstone TC, Wang F, Lin W, Zheng Y-R, Page JE, Hemann MT, Lippard SJ (2015) Necroptosis-inducing rhenium(V) oxo complexes. J Am Chem Soc 137:2967–2974 [PubMed: 25698398]

28. Ginsburg O, Bray F, Coleman MP, Vanderpuye V, Eniu A, Kotha SR, Sarker M, Huong TT, Allemani C, Dvaladze A, Gralow J, Yeates K, Taylor C, Oomman N, Krishnan S, Sullivan R, Kombe D, Blas MM, Parham G, Kassami N, Conteh L. The global burden of women's cancers: a grand challenge in global health (www.thelancet.com Published online November 1, 2016). 10.1016/S0140-6736(16)31392-7.

29. Cancer deaths among women to rise 60% by 2030, new reports warn. The Guardian, 11 1, 2016

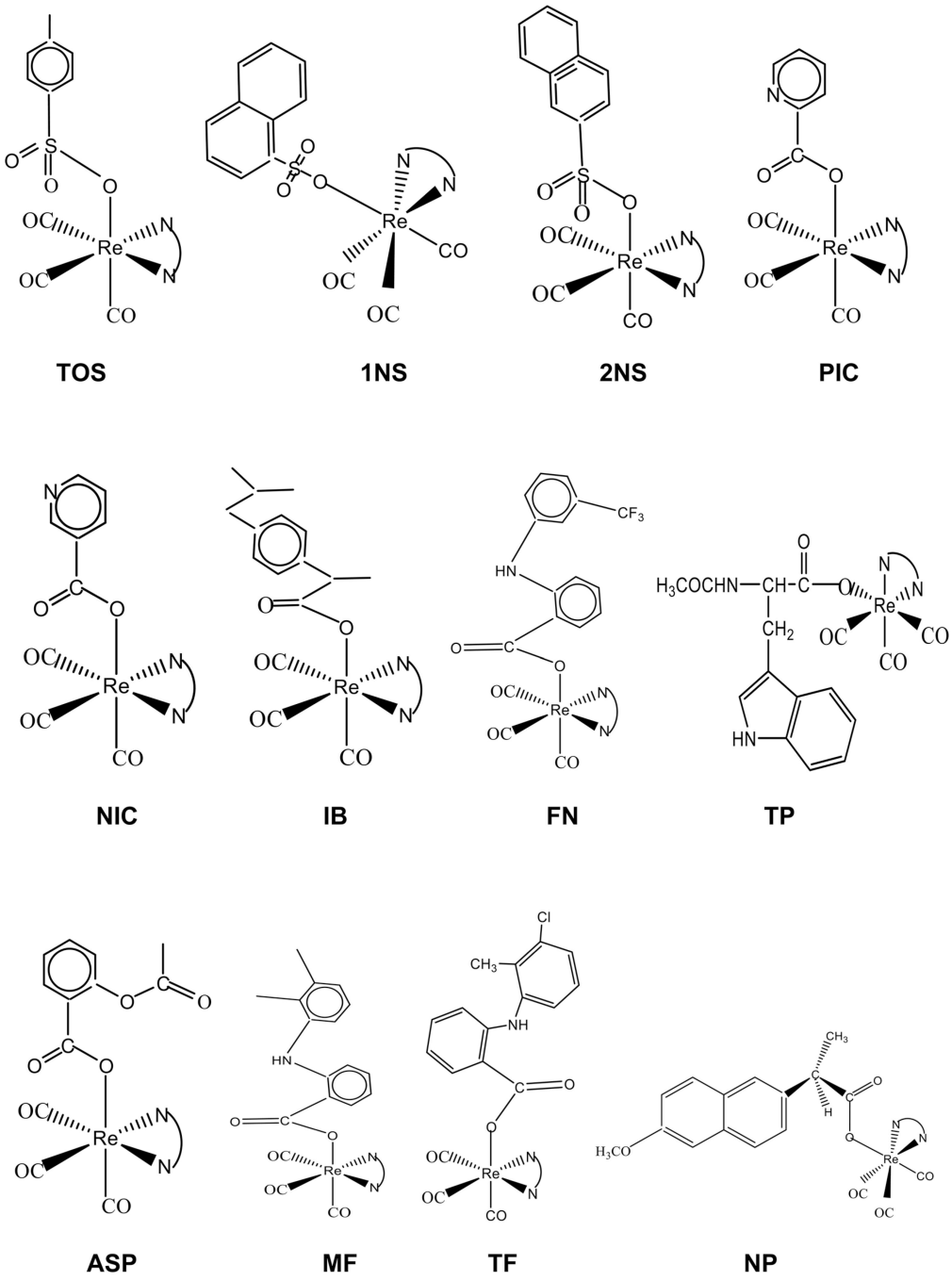

Fig. 1.
Structural formulas for 12 series of organorhenium compounds

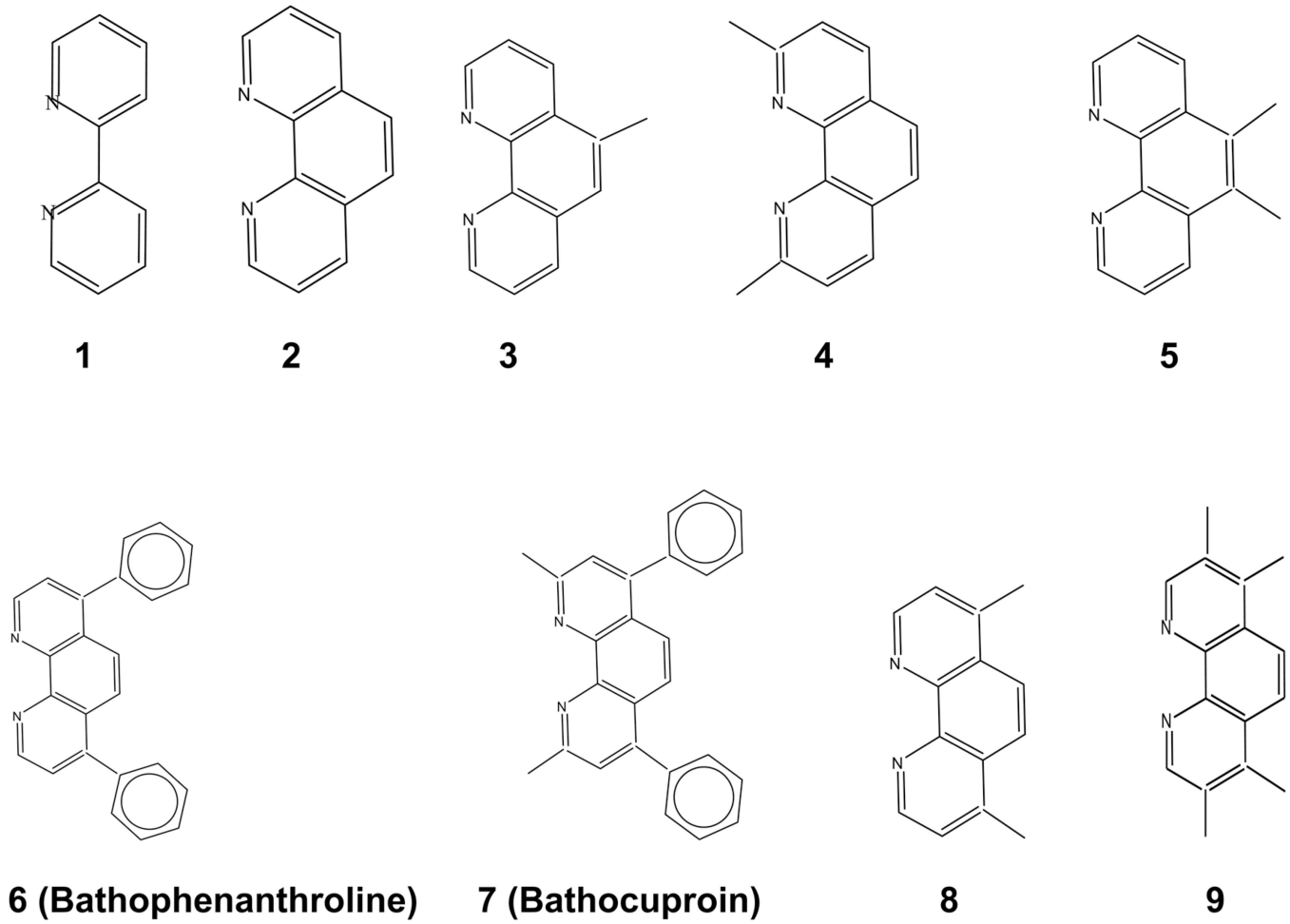

Fig. 2.
Structural formulas for the nitrogen-containing ligands N⁀N

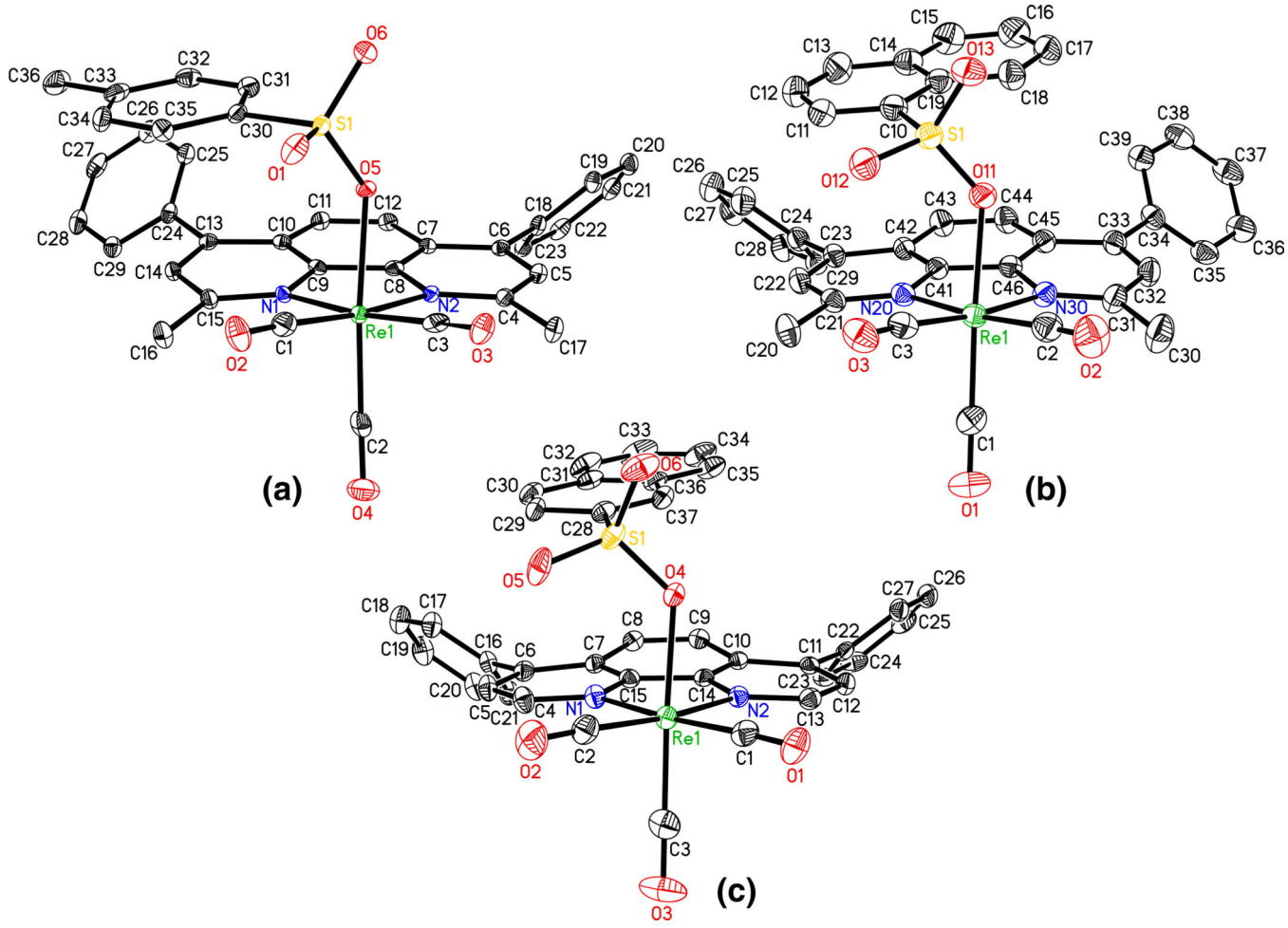

Fig. 3.

X-ray structures of **TOS7** (**a**), **1NS7** (**b**), and **2NS6** (**c**) showing planarity of the polypyridyl ligands

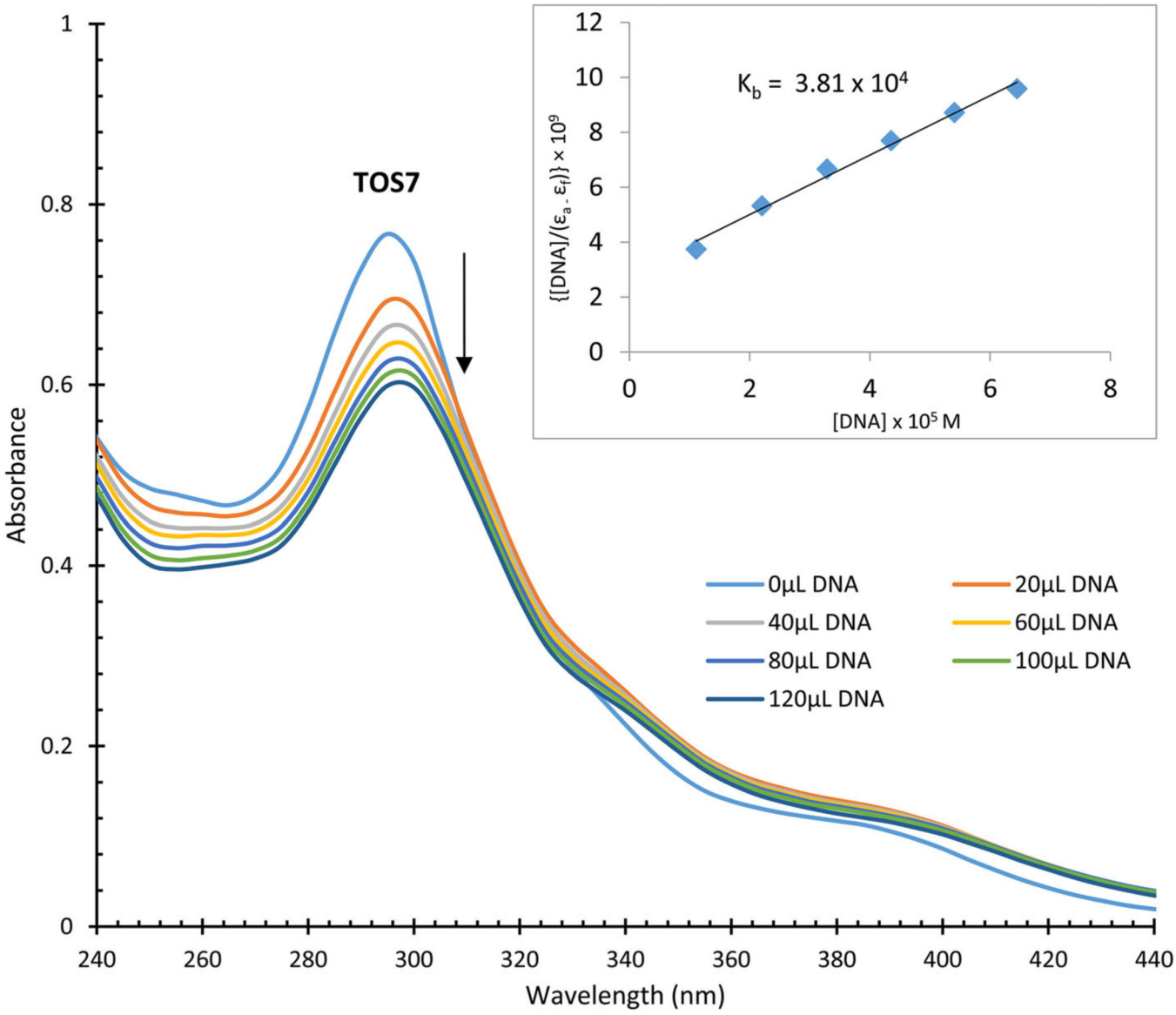

Fig. 4.

Absorption spectra for the titration of 25 µM of **TOS7** in the absence and presence of varied amounts of DNA. Stock [DNA] = 1693 µM

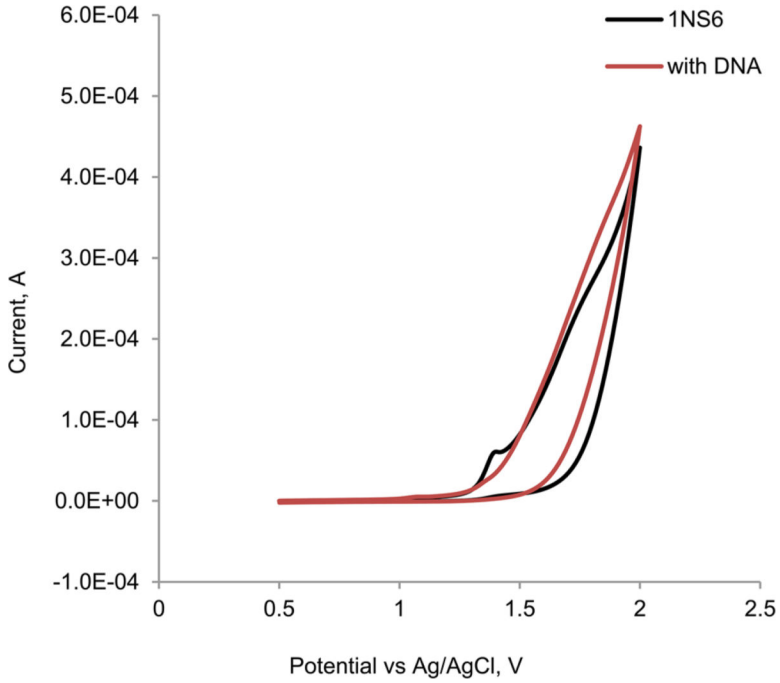

Fig. 5.

Cyclic voltammogram of 0.7 mM **1NS6** in the absence and presence of 0.1 mM DNA

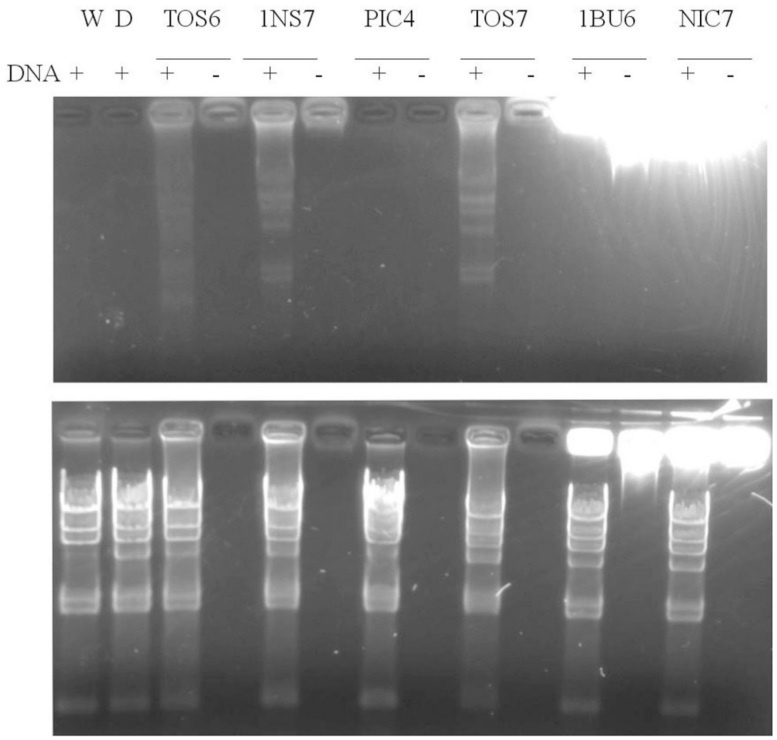

Fig. 6.

Gel electrophoresis DNA-binding assay. The compounds dissolved in DMSO/water in the presence or absence of lambda *Hin*dIII DNA markers and incubated at room temperature for 1 h. The samples electrophoresed and imaged under broad band UV light prior to (top panel) and after counterstaining with EB (bottom panel)

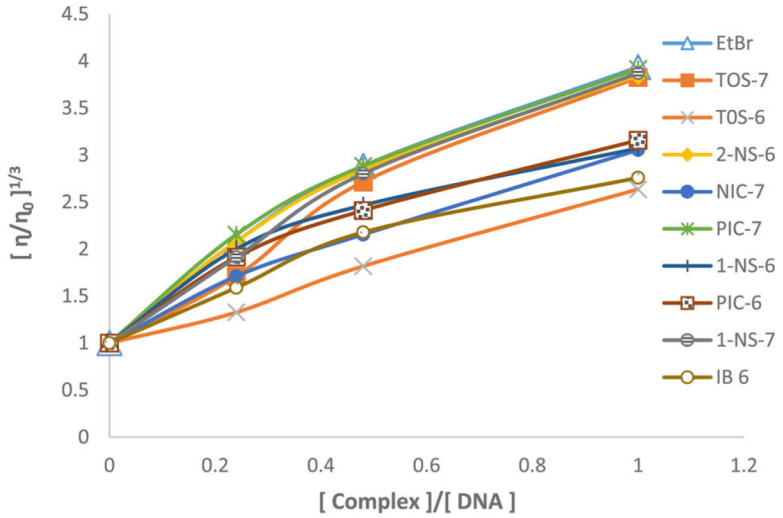

Fig. 7.

Relative viscosity $(\eta/\eta_o)^{1/3}$ of CT-DNA (0.2 mM) in buffer solution (5 mM KH_2PO_4 and 4 mM NaCl at pH 7.2) in the presence of increasing amount of complexes and EB (r = [complex]/[DNA])

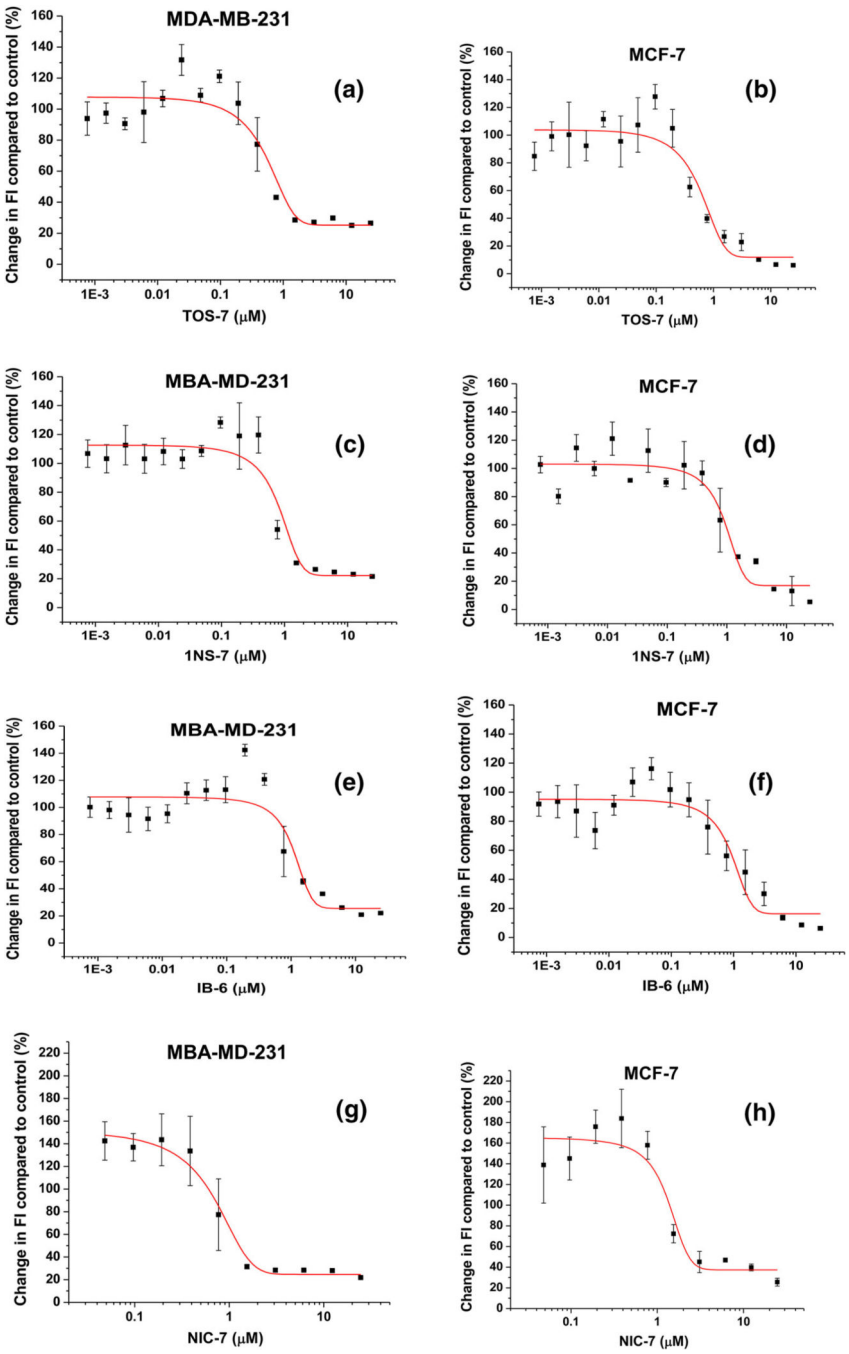

Fig. 8.

Changes in fluorescence intensity after 72-h treatment of MCF-7 and MDA-MB-231 breast cancer cells with various concentrations of four compounds—graphs for **TOS7**: **a**, **b**, **1NS7**: **c**, **d**, **IB6**: **e**, **f**, **NIC7**: **g**, **h**

Table 1

The IC_{50} values (in μM) of potent organorhenium complexes on breast cancer cells

Compound IC50		MCF-7A error (±)	MCF-10A IC50	Error (±)	Compound IC50		MDA-MB-231 error (±)
TOS7	0.337	0.303	1.78	0.173	TOS7	0.248	0.336
PIC4	0.425	0.226	0.023	0.002	NIC7	0.591	0.145
1NS7	0.849	0.255	2.51	0.187	1NS7	0.716	0.242
IB6	0.958	0.261	1.47	0.177	PIC7	1.03	0.181
1B4	1.25	0.607	12.1	0.554	IB6	1.06	0.375
TOS6	1.27	0.228	3.46	0.186	2NS6	1.08	0.198
2NS6	1.31	0.297	2.79	0.250	PIC6	1.23	0.197
NIC7	1.33	0.29	6.38	0.316	TOS6	1.27	0.361
PIC6	1.51	0.243	3.02	0.133	1NS6	1.53	0.143
1NS4	1.54	0.179	1.59	0.351	FN4	1.7	0.314
TOS4	1.55	0.285	5.7	0.337	TP7	1.74	0.140
FN4	1.56	0.420	2.65	0.253	2NS4	1.86	0.318
2NS4	1.58	0.263	1.66	0.229	TP6	1.99	0.341
PIC7	1.65	0.171	6.31	0.240	ASP7	2.41	0.328
1NS6	1.7	0.226	3.63	0.403	TP4	2.59	0.472
FNS	1.89	0.313	11.1	1.88	1NS4	2.78	0.373
2NS5	2.11	0.267	6.32	0.157	NIC4	2.97	0.172
IB5	2.55	0.673	3.37	0.406	ASP4	3.01	0.252
MF4	2.61	0.496	NA		TOS4	3.09	0.284
1B2	2.69	0.334	12.1	0.298	FN6	3.27	0.212
FN6	2.75	0.315	3.68	0.299	TOSS	3.55	0.537
FN5	2.8	0.267	6.09	0.397	NIC8	3.58	0.331
2N58	2.83	0.516	1.51	0.201	NIC3	3.64	0.625
NIC4	2.93	0.363	5.83	0.264	NIC6	4.24	0.212
MF2	2.95	0.314	12.1	0.287	2N58	5.4	1.02
NIC8	2.98	0.535	5.62	0.248	ASPS	5.76	0.271
TP7	2.98	0.292	3.04	0.431	ASP9	6.02	0.289
1N52	3.09	0.528	11.6	0.872	2N55	6.04	0.204

Compound IC50		MCF-7A error (±)	MCF-10A IC50	Error (±)	Compound IC50		MDA-MB-231 error (±)
ASP9	3.11	0.403	6.48	0.318	TF6	6.08	0.357
TP8	3.11	0.376	12.3	0.368	1NS3	6.11	0.601
TOSS	3.12	0.399	6.08	0.143	IB4	6.17	0.767
IB3	3.16	0.406	12.1	0.263	PIC8	6.18	0.164
TOS2	3.24	0.557	6.75	0.444	FN3	6.33	0.494
NIC8	3.25	0.482	6.08	0.160	2N57	6.34	0.486
MF1	3.27	0.473	12.9	0.514	TP5	6.39	0.505
1NS3	3.29	0.517	6.08	0.357	PIC4	6.39	0.362
NIC1	3.37	0.992	>24		ASPS	6.41	0.261
PIC8	3.39	0.353	6.36	0.135	TF8	6.44	0.388
PIC2	3.51	0.410	11.7	0.347	IBS	6.47	0.736
ASP2	3.54	0.487	12.2	0.237	NP6	6.48	0.577
NIC6	3.57	0.988	7.16	1.29	NIC8	6.48	0.187
TOS8	3.61	0.418	6.27	0.186	NP7	6.52	0.384
TF8	3.7	0.383	12.1	0.453	PIC8	6.53	0.467
MF3	4.17	1.45	12	0.374	TOS8	6.54	0.269

NA: not active